A Status Review of the Commercial Supersonic Technology (CST) Aeroservoelasticity (ASE) Project

Walter A. Silva,* Mark D. Sanetrik,† Pawel Chwalowski,‡ Christy Funk,§
Donald F. Keller¶

NASA Langley Research Center, Hampton, Virginia

Ulf Ringertz‖

Kungliga Tekniska Högskolan, or Royal Institute of Technology, Stockholm, Sweden

An overview of recent progress regarding the computational aeroelastic and aeroservoelastic (ASE) analyses of a low-boom supersonic configuration is presented. The overview includes details of the computational models developed to date with a focus on unstructured CFD grids, computational aeroelastic analyses, sonic boom propagation studies that include static aeroelastic effects, and gust loads analyses. In addition, flutter boundaries using aeroelastic Reduced-Order Models (ROMs) are presented at various Mach numbers of interest. Details regarding a collaboration with the Royal Institute of Technology (KTH, Stockholm, Sweden) to design, fabricate, and test a full-span aeroelastic wind-tunnel model are also presented.

I. Introduction

The unique structural configuration of supersonic aircraft combined with nonlinear aerodynamics and rigid-body effects often results in highly complex nonlinear aeroelastic/flight

*Senior Research Scientist, Aeroelasticity Branch, AIAA Associate Fellow.
†Aerospace Engineer, Aeroelasticity Branch, AIAA Senior Member .
‡Aerospace Engineer, Aeroelasticity Branch.
§Aerospace Engineer, Aeroelasticity Branch.
¶Aerospace Engineer, Aeroelasticity Branch.
‖Professor, Department of Aeronautical and Vehicle Engineering, AIAA Senior Member

dynamics phenomena. These aeroelastic phenomena can affect ride quality, gust loads, flutter, flight dynamics and control, and engine performance. The aeroelastic/flight dynamics phenomena simultaneously influence the airframe and propulsion system controls, producing undesirable effects on performance and flying characteristics.

These aeroservoelastic (ASE) phenomena need to be thoroughly understood in order for supersonic flight to be safe, efficient, and comfortable. In addition, there is an opportunity, through active controls, to exploit these phenomena for improved performance and efficiency. Analysis and design capabilities for slender supersonic aircraft may then be enhanced by including this new knowledge.

Under the auspices of the Supersonics Project under NASA's Fundamental Aeronautics Program (FAP), the SemiSpan SuperSonic Transport (S4T) was the subject of four experiments in the NASA Langley Transonic Dynamics Tunnel (TDT): two open-loop (no feedback control) tests and two closed-loop (with feedback control) tests over the span of three years between 2007 and 2010. A special session on the various aspects of the S4T program was organized for the AIAA Structures, Structural Dynamics, and Materials (SDM) conference held in 2012. The work involving the S4T was completed in 2012.

The Supersonics Project was renamed the High Speed Project and, more recently, the Commercial Supersonic Technology (CST) Project. The CST Project continues the original charter of the Supersonics Project, addressing the technical barriers to safe, efficient, and economical supersonic flight. One of the efforts within the High Speed Project is the ASE element, tasked with addressing the aeroelastic (AE), ASE, and aeropropulsoservoelastic (APSE) challenges associated with low-boom supersonic configurations. In order to address more realistic challenges associated with a full-span configuration, including rigid-body modes, the CST ASE element is now focusing on a full-span low-boom configuration.

A top priority for the CST ASE element is to develop the tools required to perform accurate, high fidelity computational AE, ASE, and APSE analyses in support of the design of future low-boom high speed civil aircraft. As a means of accomplishing that priority, the CST Project collaborated with Lockheed-Martin to conduct such analyses. Under the NASA N+2 (two generations from present state) contract, Lockheed-Martin developed a low-boom supersonic configuration and a detailed finite element model (FEM). An artist rendering of the Lockheed-Martin N+2 configuration is presented in Figure 1.

Figure 1: Artist's concept of the Lockheed-Martin N+2 configuration.

This paper presents a status update on this computational effort [1–3]. This includes a brief description of the N+2 configuration, the finite element model (FEM), computational aeroelasticity solutions, and sonic boom propagation results that include static aeroelastic effects. Gust loads analyses of the N+2 configuration will also be presented. Finally, a summary of the work being performed in the area of Reduced-Order Model (ROM) development and application will also be discussed.

II. Unstructured Grids

Unstructured grids of the N+2 configuration have been generated for use with the FUN3D code [4]. Additional details regarding the aeroelastic capability within the FUN3D code can be found in the reference [5].

Recent work has focused on the creation of improved grids that are better suited for sonic boom propagation. Given that the grids generally used for aeroelastic analyses are not well suited for modeling sonic boom propagation, several parametric studies have been performed in order to develop the best possible grids for both aeroelastic and sonic boom propagation analyses. Presented in Figure 2 is a close-up detail of the grid used for standard computational aeroelastic analyses. As can be seen, the generation of a grid for aeroelastic analysis does not, typically, include tailoring the grid to capture supersonic bow shocks. Generally speaking, a grid generated for computational aeroelastic analyses can be used for computing solutions at multiple Mach numbers. Given that the primary focus of the aeroelastic analyses is the unsteady surface pressures and the resultant integrated forces, the

emphasis of the quality of the grid is focused on the surface of the vehicle and not on the accurate propagation of any bow shocks.

Grids for sonic boom prediction are aligned to the Mach angle and stretched to reduce dissipation so that pressure signatures can be computed off-body. The off-body signatures are then processed using the sonic boom propagation software sBOOM [6] to compute the propagation of the off-body signature to the ground level.

It is also important to mention that the sonic boom propagation results presented below are preliminary. The initial goal of this effort was to implement a sonic boom propagation method using FUN3D to include the effects of static aeroelastic deformation. This method currently does not include any trim conditions for the vehicle nor does it include the computation of the static aeroelastic deformation from a vehicle jig shape. The latter limitation is currently being developed and will be presented in a future publication while the former will depend on future enhancements to the FUN3D code.

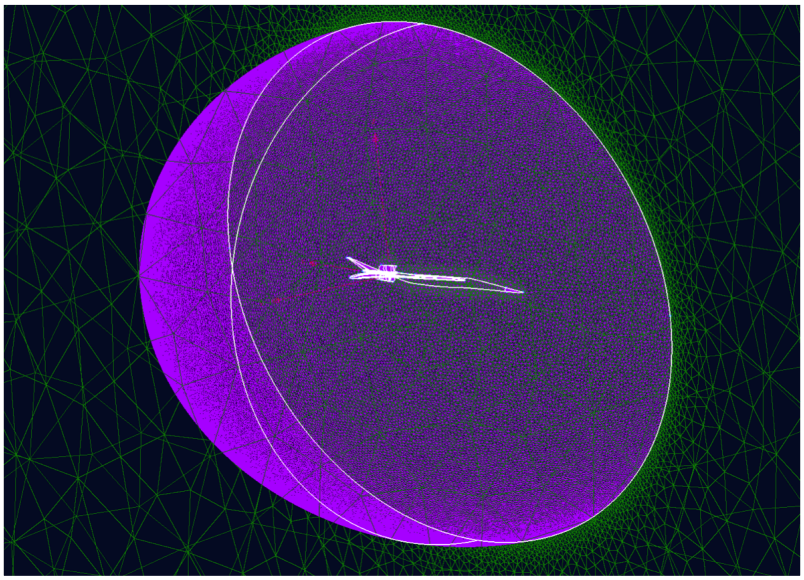

Figure 2: Close-up of the grid used for aeroelastic analyses.

Figure 3 shows the steady aerodynamic flow computed using the conventional aeroelastic analysis grid at a Mach number of 1.7 and angle of attack of 2.25 degrees. As can be seen, the bow shocks are not well resolved for this solution even with the use of a grid with approximately 12 million grid points. Clearly, the grids that are typically used for computational aeroelastic analysis are not appropriate for the computation of the effect of static aeroelastic response on sonic boom propagation. For this type of analyses, it is appropriate to generate grids suitable for computing the propagation of the sonic boom and then use these grids for computational aeroelastic analyses.

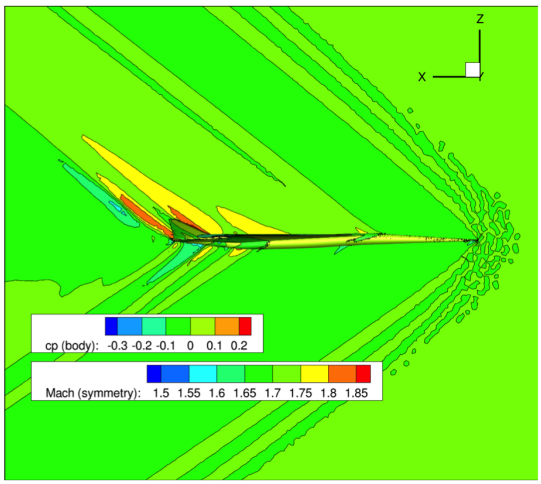

Figure 3: Steady aerodynamic solution for sonic boom propagation analysis using grid generated for aeroelastic analyses.

Multiple grids were generated for sonic boom propagation studies with grid dimensions of 16 million grid points (coarse), 45 million grid points (medium), and 90 million grid points (fine). An additional variation considered the effect of the engines on both the sonic boom propagation and the aeroelastic response. The engine masses are, of course, still included in the structural dynamic model of the vehicle. The results presented in the remainder of this section consist of computations at the cruise condition (Mach number of 1.7 and alpha = 2.25 degrees) using grids that were generated without the engines.

Presented in Figure 4 is the static aeroelastic deformation of the entire vehicle at the cruise condition due to an inviscid aerodynamic solution. Although the deformation is not large, it can be seen that it does occur over a large portion of the vehicle. This will have an impact on the sonic boom propagation.

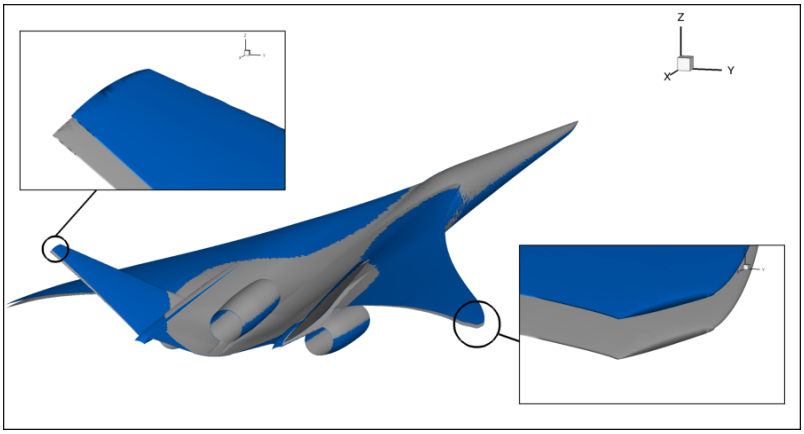

Figure 4: Static aeroelastic deformation of the N+2 configuration at cruise. Gray is undeformed; Blue is deformed.

Figure 5 presents the coarse grid used for sonic boom propagation. The challenge in generating grids for sonic boom propagation analyses is that a separate grid needs to be generated for each condition of interest (Mach number and angle of attack). This complexity adds significant overhead to the overall analysis, but is essential for obtaining accurate results. Subsequent computational aeroelastic analyses are then performed using each one of the sonic boom propagation grids.

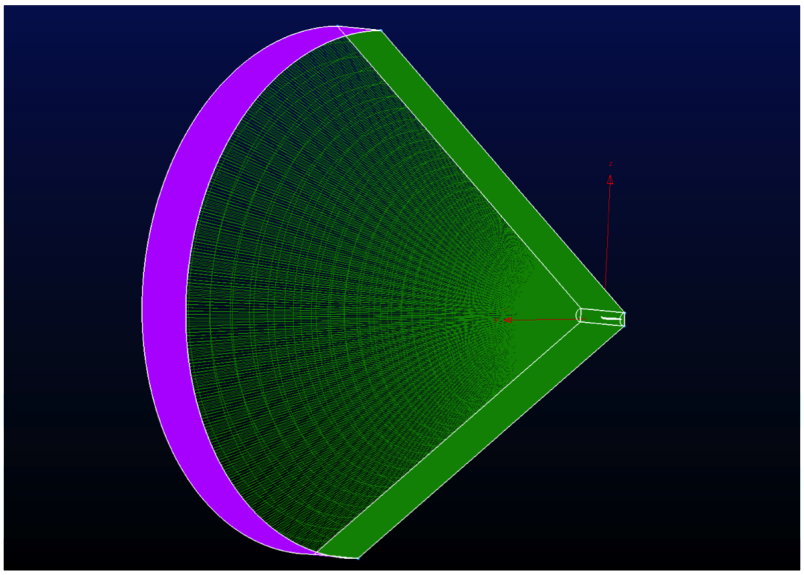

Figure 5: Sample coarse grid used for conducting a sonic boom propagation analysis.

Figure 6 shows the steady aerodynamic flow Mach number at the cruise condition determined using the coarse sonic boom grid without the engines. As can be seen, the bow shocks are better resolved using this grid compared to the grid generated for aeroelastic analyses. Presented in Figure 7 is a close-up view of Figure 6 showing the improved resolution of the bow shocks.

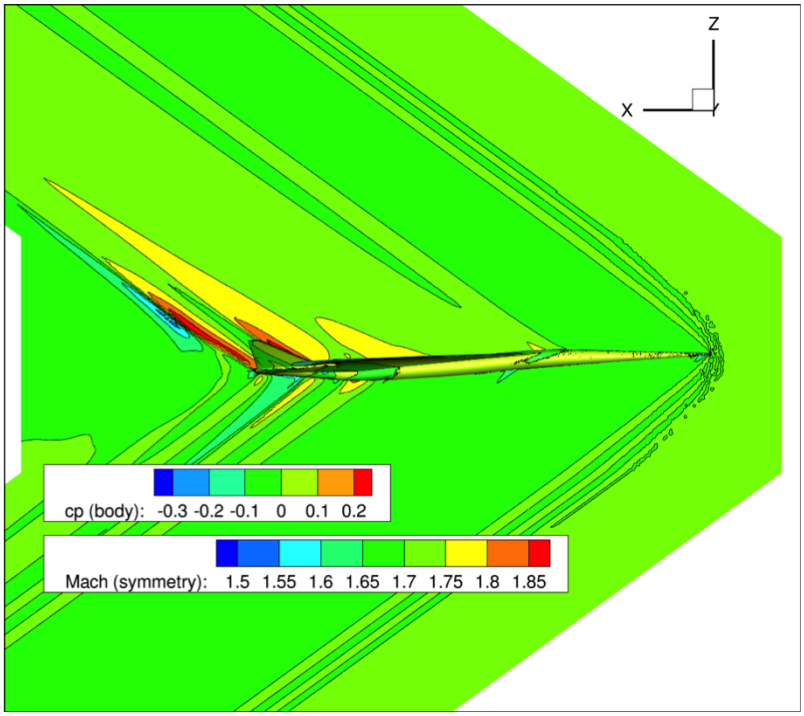

Figure 6: Steady aerodynamic solution for sonic boom propagation analysis using the coarse grid.

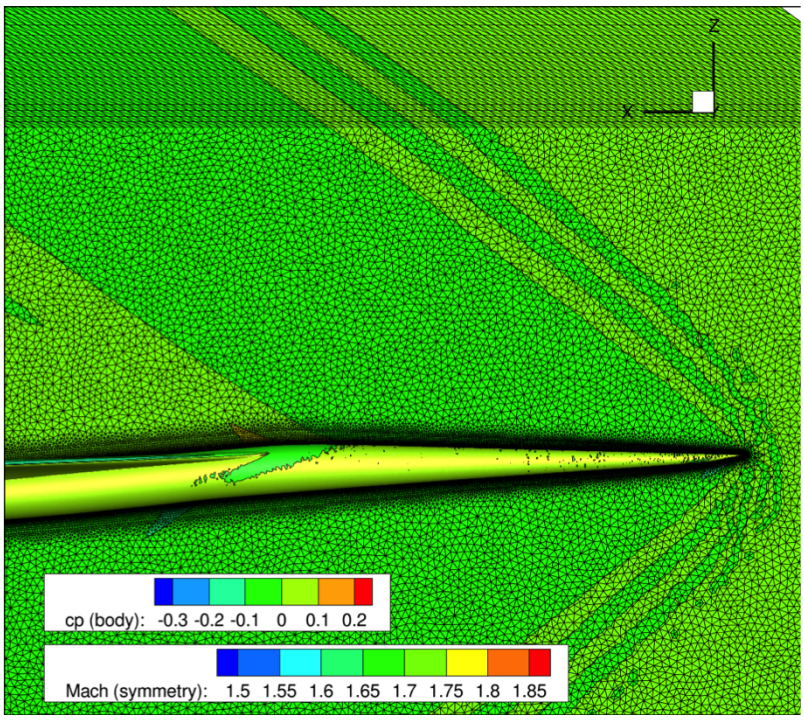

Figure 7: Close-up detail of the bow shocks for sonic boom analysis using the coarse grid.

Shown in Figure 8 and in Figure 9 is the steady aerodynamic flow Mach number at the

cruise condition using the medium and fine sonic boom grids, respectively, both without the engines. Clearly, resolution of the grid significantly improves the resolution of the bow shocks which leads to improved accuracy with respect to sonic boom propagation.

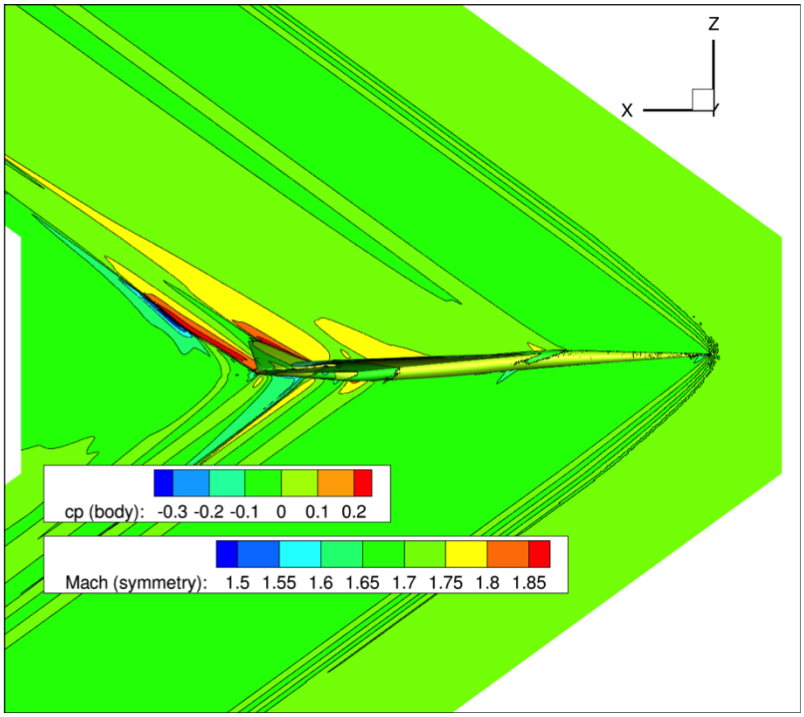

Figure 8: Steady aerodynamic solution for sonic boom propagation analysis using the medium grid.

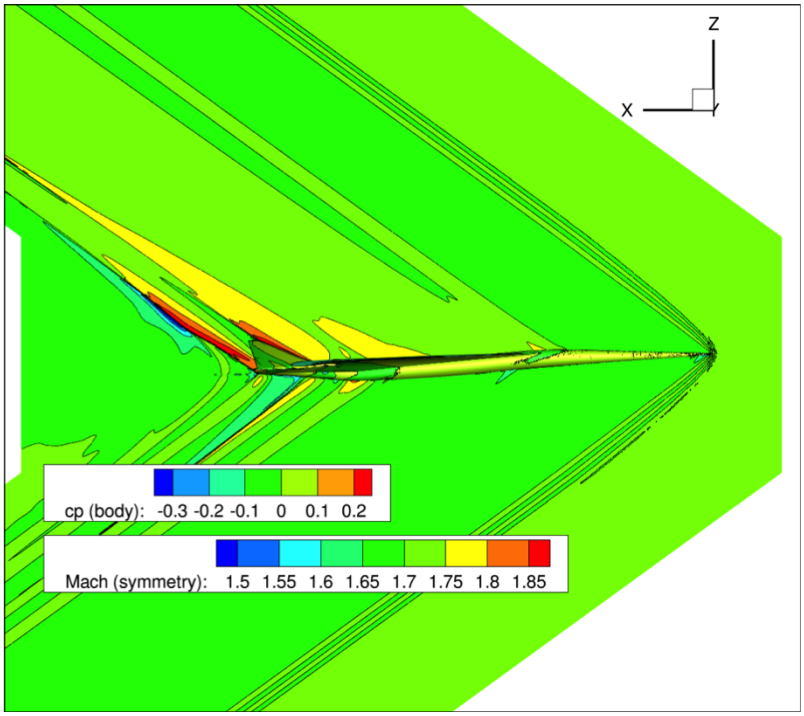

Figure 9: Fine grid (57.5 million) FUN3D steady (undeformed) Euler (inviscid) result at cruise condition.

Figure 10 presents a comparison of the ground level boom signature for the three different grid densities for the configuration with no engines at the cruise condition. As can be seen, use of the finer grid exhibits some variation near the middle of the signature not seen with the coarse and medium density grids.

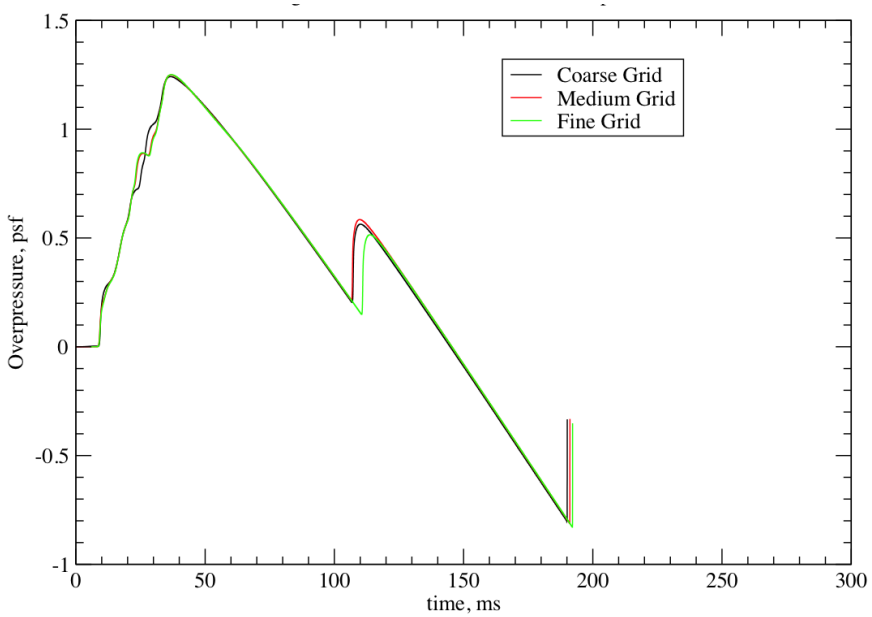

Figure 10: Ground-level boom signature at cruise for various grid densities.

Presented in Figure 11 is a comparison of the ground-level boom signature for the undeformed configurations, with and without engines at the cruise condition. As can be seen, inclusion of the engines in the aerodynamic solution clearly exhibits some variation near the middle of the signature. This difference is not surprising and is intended to serve as a basis for comparison with the deformed configuration (with and without engines), to be presented in a subsequent paper.

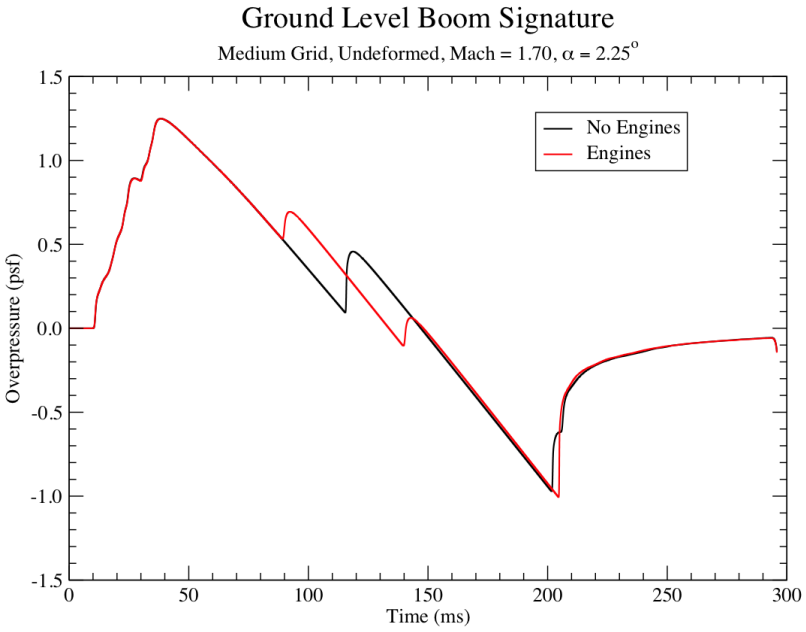

Figure 11: Effect of engine presence on ground-level boom signature at cruise, undeformed case, medium grid.

Presented in Figure 12 is a comparison of the ground-level boom signature for the undeformed and deformed conditions for the configuration with no engines at the cruise condition. There is clearly an effect of the static aeroelastic deflection on the ground-level boom signature. However, additional analysis is required to better understand the implications of this result.

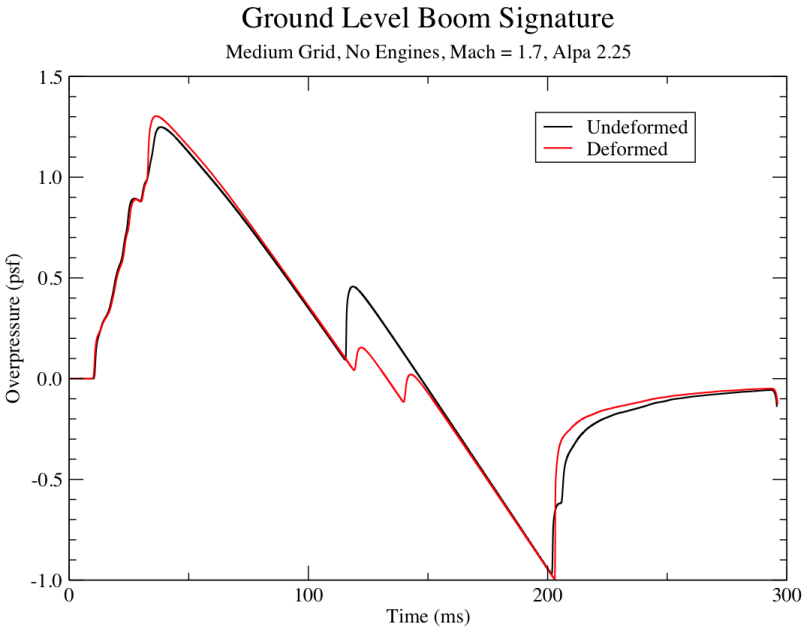

Figure 12: Ground-level boom signature at cruise for the undeformed and deformed cases.

The following figures present a comparison of the near-field pressure signatures and the corresponding sonic boom ground signatures for a viscous vs. inviscid solutions and for viscous rigid vs. deformed solutions. All computations were performed for the beginning of cruise condition (Mach = 1.70, alpha = 2.25 degrees, altitude 48,400 ft, Re = 2.15e+06/ft (179,00/in)). The inviscid solution has a wall spacing of 0.1in and 22.5e+06 grid points; the viscous solutions have a wall spacing of 0.0001in and 28.5e+06 grid points. The near-filed pressure signatures were extracted 3 body lengths below the aircraft.

Figure 13 presents a comparison of near-field pressure signatures for rigid inviscid versus rigid viscous solutions. It appears that, at this cruise condition, the pressure differences appear to be slightly larger for the viscous solution. However, the sonic boom ground signature for these two solutions, presented in Figure 14, show only a modest variation in the signatures.

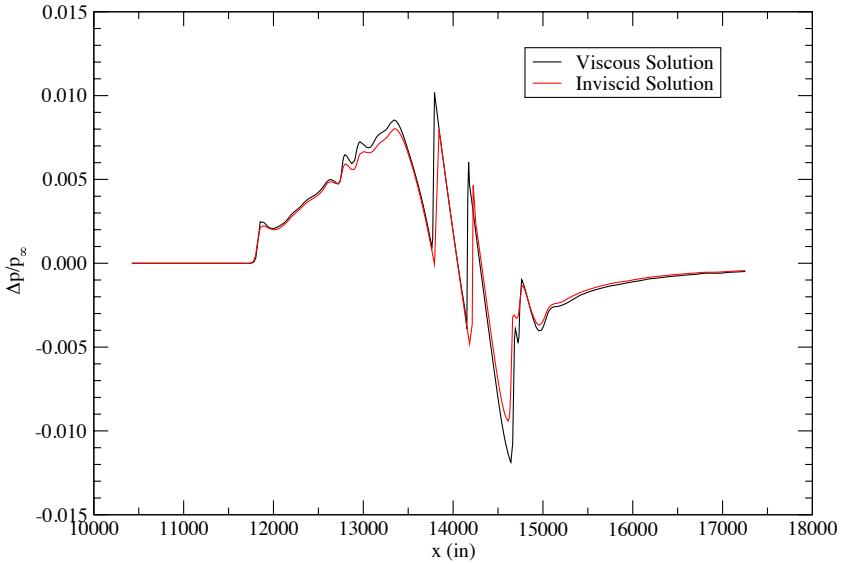

Figure 13: Comparison of near-field pressure signatures for inviscid and viscous solutions.

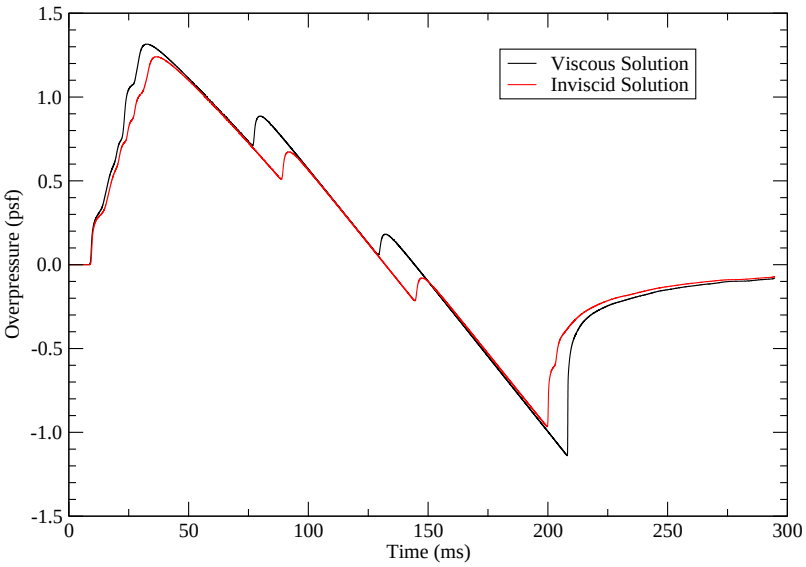

Figure 14: Comparison of sonic boom ground signatures for inviscid and viscous solutions.

Similarly, Figure 15 and Figure 16 present the near-field pressure signatures and corre-

sponding sonic boom ground signatures for the viscous rigid and flexible solutions. Again, at this cruise condition, there are some differences, but these differences also appear to be slight. Additional research is currently underway to further evaluate these results and perform additional parametric variations.

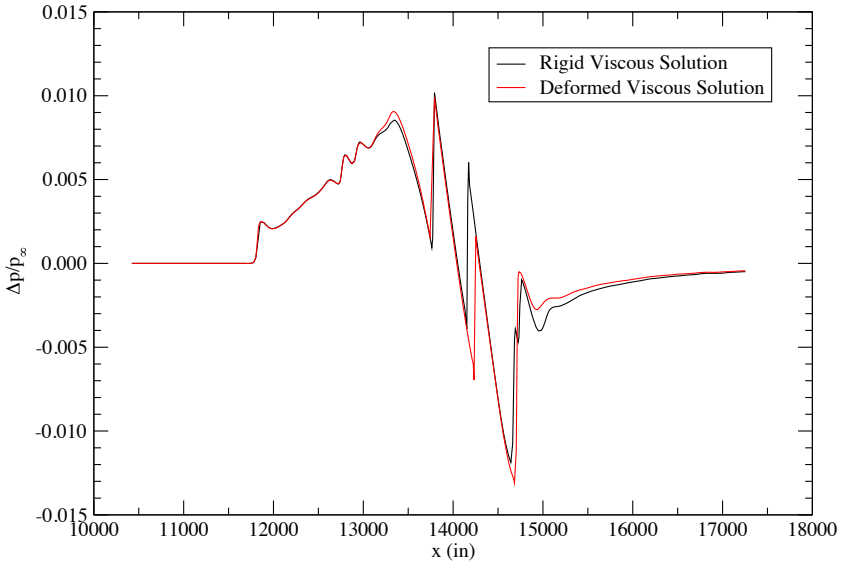

Figure 15: Comparison of near-field pressure signatures for viscous rigid and flexible solutions.

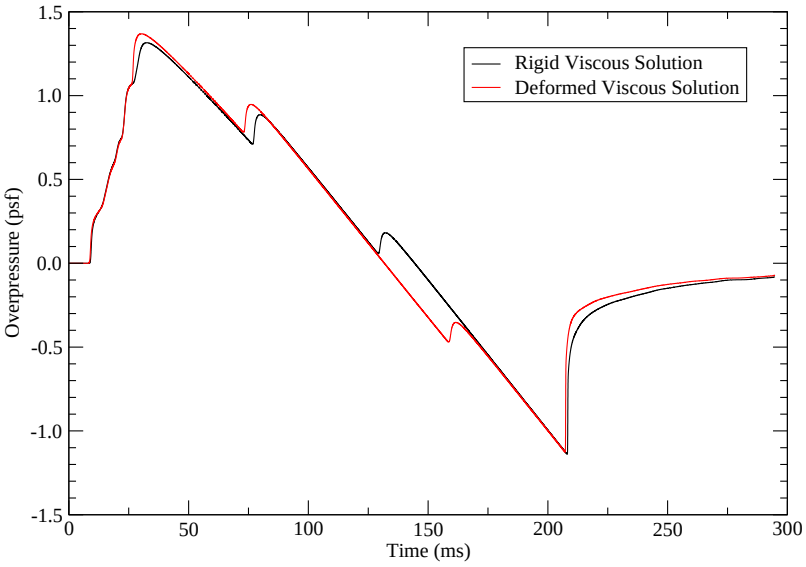

Figure 16: Comparison of sonic boom ground signatures for viscous rigid and flexible solutions.

The computation of a realistic static aeroelastic deformation involves starting the deformation computation from an optimal undeformed shape that will then deform into the optimal cruise shape. This process is known as jig-shape optimization. Given the complexities of performing an optimization procedure to compute a true jig shape, in the following an approximate method is applied in order to compute a very crude estimate of what will be referred to as a jig shape of the vehicle. A method for computing this approximate jig shape consists of the following process. Starting from the rigid (not jig shape) condition, a static aeroelastic deformation is computed. This deformation is then inverted (multiply by -1) and treated as an approximate jig shape. A new static aeroelastic deformation is then computed starting from this approximate jig shape. Subsequent iterations may be performed in order to get the final static aeroelastic deformation as close to the design (rigid) shape as possible.

Presented in Figure 17 is an image that presents the results obtained when computing an approximate jig shape for the N+2 configuration. The original (rigid) shape is presented as the gray surface. A static aeroelastic deformation is computed starting from this condition, presented as the blue surface. This deformation is then inverted (multiplied by -1) in order to create an approximate jig shape (green surface). A new static aeroelastic deformation is then computed that starts from this approximate jig shape, resulting in the purple surface. As can be seen, the purple surface is close to the gray surface but some additional iterations may be

required in order to improve the matching of these two surfaces. Figure 18 presents results of the same process but for the tail tip. The impact of this calculation on the propagation of the sonic boom is currently underway and will be presented in a subsequent paper.

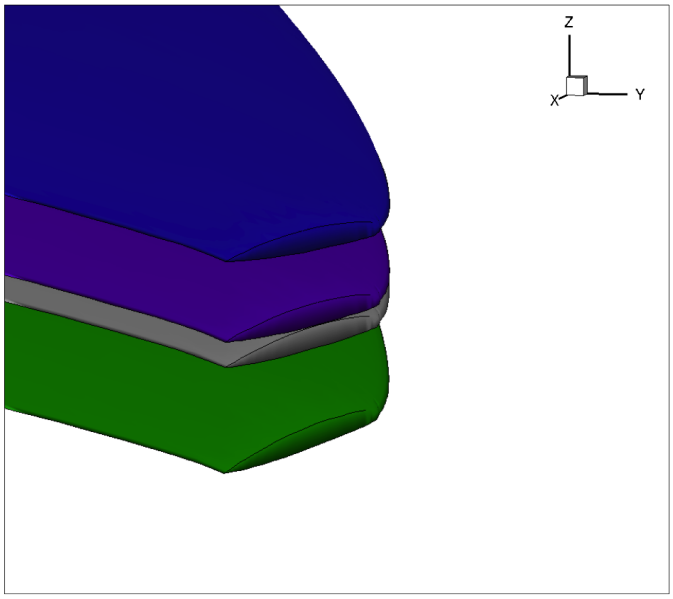

Figure 17: Computation of the jig shape using FUN3D, wing tip view, showing the rigid (gray), initial deformation (blue), inverse deformation or approximate jig shape (green), and final deformation from approximate jig shape (purple).

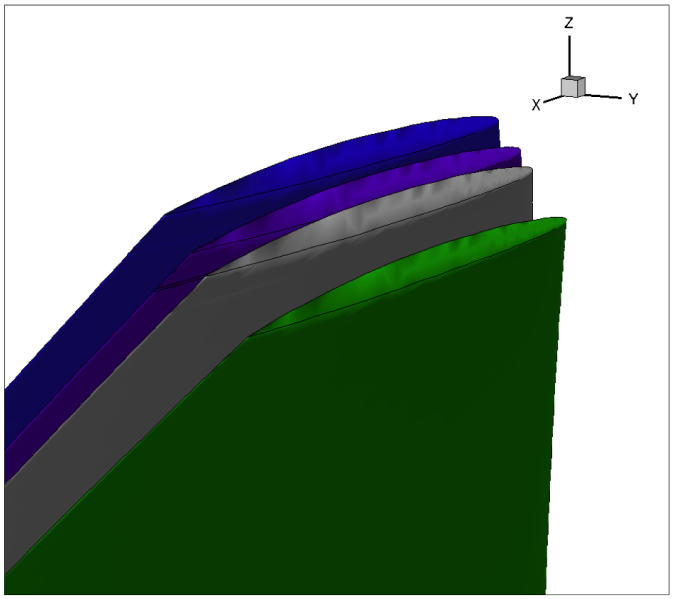

Figure 18: Computation of the jig shape using FUN3D, tail tip view, showing the rigid (gray), initial deformation (blue), inverse deformation or approximate jig shape (green), and final deformation from approximate jig shape (purple).

III. Reduced-Order Models

The goal behind the development of a ROM for the rapid computation of unsteady aerodynamic and aeroelastic responses is aimed at addressing two challenges. The first challenge is the computational cost associated with full CFD aeroelastic simulations, which increases with the fidelity of the nonlinear aerodynamic equations to be solved as well as the complexity of the configuration. Computational cost, however, may be reduced via the implementation of parallel processing techniques, advanced algorithms, and improved computer hardware processing speeds.

The second, more serious, challenge is that the information generated by these simulations cannot be used effectively within a preliminary design environment. Because the output of these full CFD aeroelastic simulations, such as the responses of the generalized coordinates, is not easily incorporated within a design environment, parametric variations and design studies can only be performed by trial-and-error. As a result, the integration of computational aeroelastic simulations into preliminary design activities involving disciplines such as aeroelasticity, aeroservoelasticity (ASE), and optimization continues to be a costly and impractical venture.

However, with the development of reduced-order modeling (ROM) methods [7, 8], the rapid generation of root locus plots using CFD-based unsteady aerodynamics is now available to aeroelasticians. This recently developed technology is being applied to the N+2 supersonic configuration for evaluation of aeroelastic mechanisms across several Mach numbers. A sample of some of those results is presented in the following.

Aeroelastic ROMs have been developed at a Mach number of 1.7, 1.05, and 0.98. Presented in Figure 19 is a comparison of the dynamic aeroelastic response from a full FUN3D aeroelastic solution and the ROM aeroelastic solution at a Mach number of 1.7 and a dynamic pressure of 2.149 psi where the time histories of the fourth mode generalized displacements are compared. As can be seen, the results are practically identical. Similar results are obtained for all the other modes, indicating good confidence in the ROM.

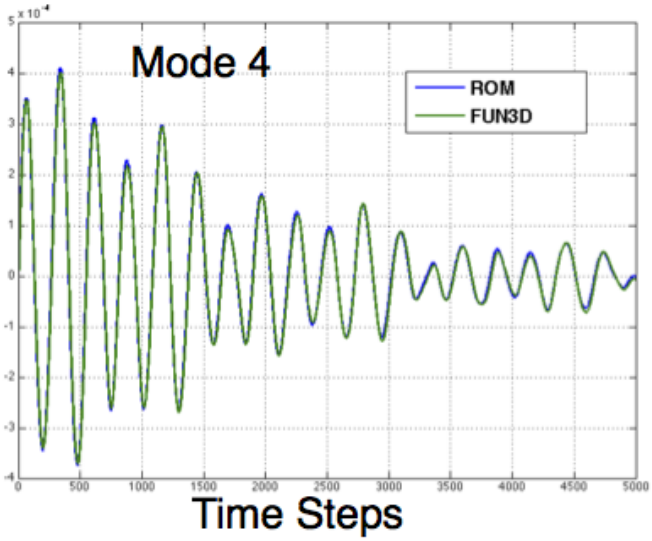

Figure 19: Comparison of full FUN3D aeroelastic response and ROM aeroelastic response for the fourth mode at M=1.7 and a dynamic pressure of 2.149 psi.

A major benefit of this ROM technology is the ability to rapidly generate an aeroelastic root locus plot that reveals the aeroelastic mechanisms occurring at that flight condition. Presented in Figure 20 is the aeroelastic root locus plot at M=0.98 with a variation in dynamic pressure from 1 to 20 psi, with the arrows indicating increasing dynamic pressure. Potential coalescence between modes is evident, including a softening of the first flexible mode. This softening of the first mode could indicate a tendency towards body freedom flutter if it couples with the short period mode. In Figure 21, the aeroelastic root locus plot at M=1.05 indicates an interesting variation of the first mode as it starts out moving in a stable direction (towards the left) and then reverses direction and moves towards the right, eventually crossing the imaginary axis (flutter). Both root loci plots have the same maximum dynamic pressure of 20 psi. The increased variation of the solution at M=1.05 indicates a greater sensitivity to flutter than at other Mach numbers thus far. Additional analyses are underway to determine the significance of this modal variation. Regardless, the flutter event is still significantly outside of the flight envelope of the N+2 configuration.

The computational cost of generating these ROM solutions consists of one full FUN3D solution that is used to generate the ROM at that Mach number. Each full FUN3D solution ran for about three hours (128 cores) and consisted of 2400 time steps. Once this solution is available, a ROM can be generated and then used to generate all the aeroelastic responses at all dynamic pressures. In comparison, a full FUN3D analysis at each dynamic pressure requires two full FUN3D solutions: a static aeroelastic (10 hours) and a dynamic aeroelastic (18 hours). Therefore, full FUN3D solutions for 20 dynamic pressures would require 560 hours (128 cores) of compute time.

In the root locus plot, each symbol represents the aeroelastic roots at a specific dynamic pressure. It is important to mention that this ROM-based root locus plot is generated in seconds while multiple full FUN3D solutions would be required for each dynamic pressure of interest to generate an equivalent full FUN3D solution root locus.

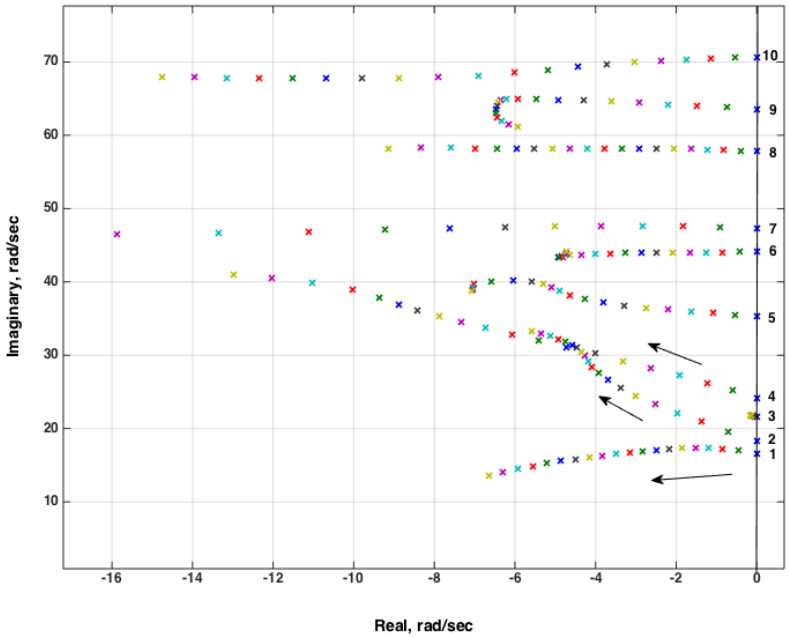

Figure 20: Aeroelastic root locus plot at M=0.98.

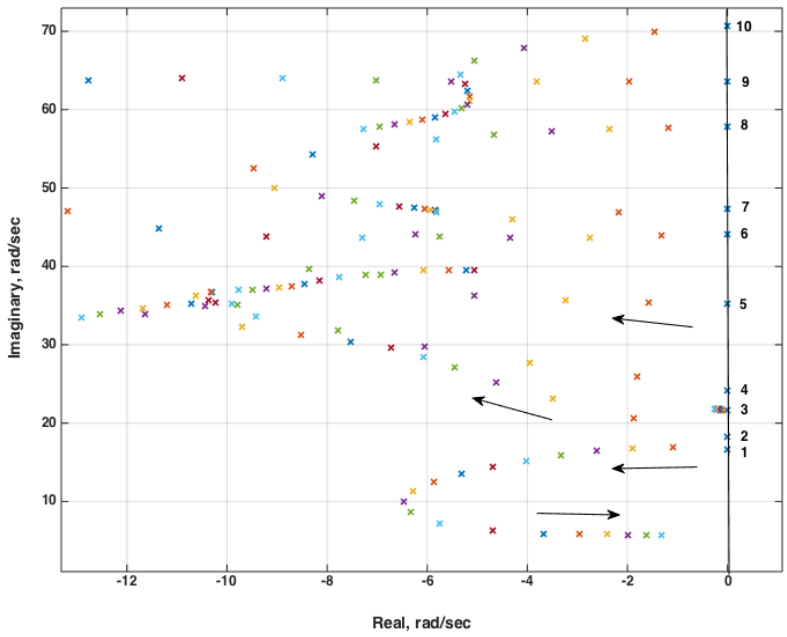

Figure 21: Aeroelastic root locus plot for the cruise condition at M=1.05.

IV. Gust Loads

An important component of any ASE analysis involves the computation of gust loads on the structure. Some preliminary gust loads analyses have been performed to determine the regions of the flight envelope that encounter the highest gust loads. This is an ongoing analysis effort but a sample of the results is presented in Figure 22. The image indicates a broad region of high stresses along the root of the wing with high stress levels also affecting the mid-fuselage section and the tail root section. It is interesting to note that loads due to gusts are not confined to the root of the wing and are predominant in the aft portions of the wing. Continued analyses are underway to determine these important regions at other flight conditions.

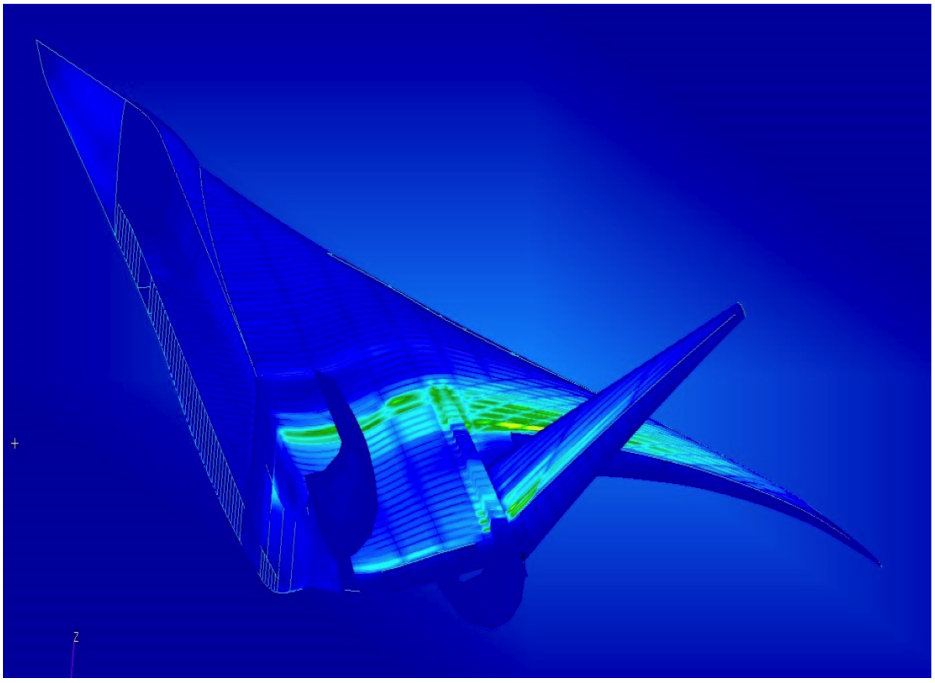

Figure 22: Regions of maximum stress due to gust loads.

V. KTH Wind-Tunnel Model and Test

There is significant interest within the aerospace community in the ability to model, analyze, and predict nonlinear aeroelastic limit cycle oscillations (LCOs). Although there is a significant amount of research being performed across several organizations in this area, a major limitation to this research is the availability of high-quality, experimental transonic LCO data [9–20].

This section presents the status of a collaborative effort between the Royal Institute of Technology (KTH) and the NASA Langley Research Center to acquire a high-quality LCO database on a full-span fighter configuration. The configuration selected will be discussed first, followed by a description of the design, fabrication process, instrumentation, and preliminary data acquired to date.

V.A. Wind-Tunnel Model Configuration

In 1985 and 1986, two wind-tunnel models of the Saab JAS 39 Gripen were designed, built, and tested in the NASA Transonic Dynamics Tunnel (TDT) for flutter clearance. One model, referred to as the stability model, was designed to be stiff but incorporated proper scaling of both the mass and geometry. The other model, referred to as the flutter model, was also designed with proper scaling of structural dynamics and was used for flutter testing with

various external stores attached.

For the current collaboration, a single generic fighter flutter-model version of these earlier models was selected. The new model, shown in Figure 23, has a similar outer mold line (OML) to the Gripen, but it has been modified to provide a more generic fighter configuration. Specifically, the air intakes were removed from the fuselage, and the wing received an aspect ratio increase and a leading-edge sweep reduction.

Figure 23: The generic fighter aeroelastic wind-tunnel model to be tested in 2016.

V.B. Data Acquisition

A significant issue associated with testing a wind-tunnel model with a large number of sensors is the routing of all the cables to a data acquisition (DAQ) system outside the tunnel test section. For the current model, approximately 100 strain gauge bridges and accelerometers are planned together with 64 pressure taps for unsteady pressure measurements. Each sensor uses 2-4 wires, resulting in several hundred wires carrying sensitive analog signals through fairly long cables, typically at least 30 meters in length, from the sensor to the data acquisition system outside the test section. This type of arrangement requires significant time in the wind tunnel to route all of the wires and cables, verify that each sensor is functioning properly via end-to-end checks, and then secure all components before the testing can begin.

In the present project, the requested test section occupation time in the TDT is limited by funding, so the model installation needs to be efficient. Fortunately, due to rapid development in computer and sensor technology, new hardware solutions have become available in much smaller sizes. There are now data acquisition systems small enough to fit inside the fuselage

of the wind-tunnel model and such a system is currently in development at KTH, as shown in Figure 24. Housing the components of the data acquisition system inside the fuselage would eliminate several of the aforementioned installation steps.

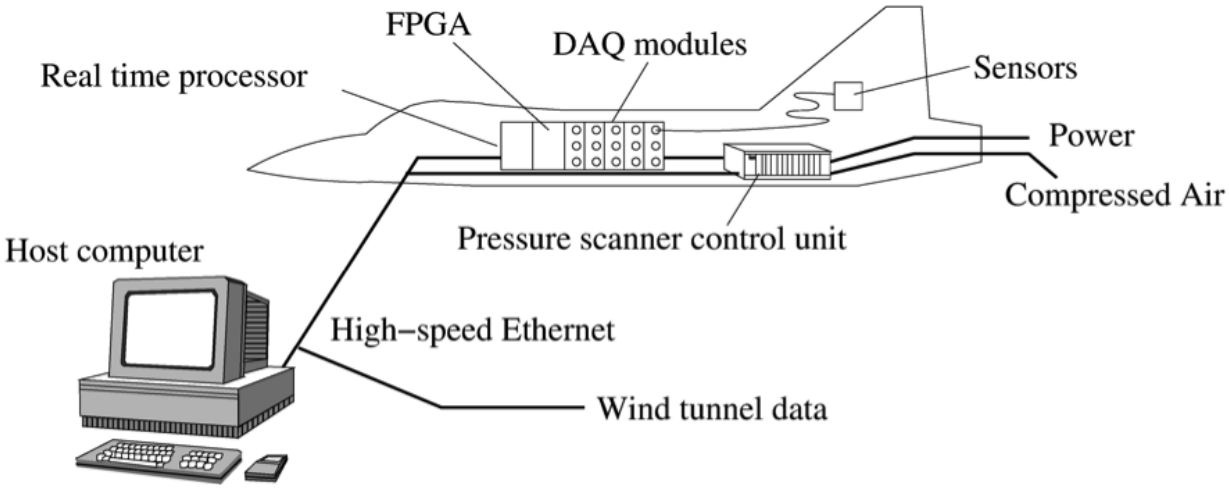

Figure 24: Measurement and control system overview. The FPGA is a field programmable gate array to faciliate data processing.

V.C. Transonic Dynamics Tunnel

Testing of the new generic fighter configuration wind-tunnel model will be conducted in the NASA Langley Transonic Dynamics Tunnel. The TDT is a unique national facility dedicated to identifying, understanding, and solving relevant aeroelastic problems. The TDT is a closed-circuit, continuous-flow, variable-pressure wind tunnel with a 16-foot square test section with cropped corners (Figure 25). The tunnel uses either air or a heavy gas as the test medium and can operate at stagnation pressures from near vacuum to atmospheric, has a Mach number range from near zero to 1.2, and is capable of achieving maximum Reynolds numbers of about 3 million per foot in air and 10 million per foot in heavy gas. Prior to 1998, the TDT used dichlorodifluoromethane, R-12, as the aerodynamic (heavy gas) test medium. The TDT now uses 1,1,1,2 -tetrafluoroethane, R-134a, as the test medium [21, 22]. Testing in heavy gas has important advantages over testing in air: improved model to full-scale similitude (which results in cheaper, heavier models with lower model elastic mode frequencies), higher Reynolds numbers, and reduced tunnel power requirements. The TDT is specially configured for flutter testing, with excellent model visibility from the control room and a rapid tunnel shutdown capability for model safety (bypass valves). Model mount systems include a sidewall turntable for semispan models, a variety of stings for full-span models and a cable-mount system for "flying" models. The TDT also offers an airstream oscillation system for gust studies, as well as digital controllers and supporting systems for

active controls testing. These capabilities make the TDT the best-suited facility in the world for flutter testing large, full-span, aeroelastically-scaled models at transonic speeds.

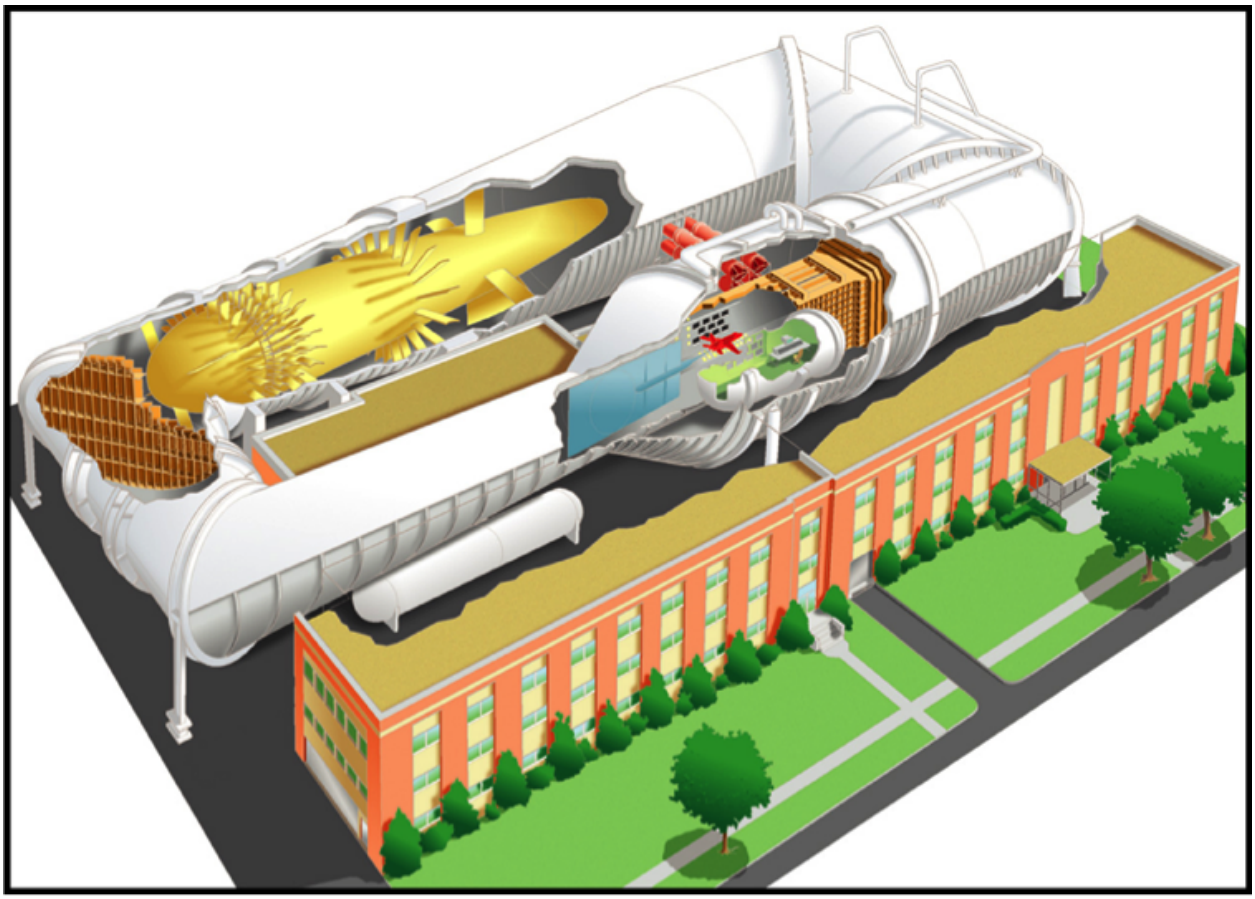

Figure 25: The Transonic Dynamics Tunnel (TDT).

V.D. CFD Grids and Analyses

Unstructured CFD grids have been generated at KTH for use with Reynolds-Averaged Navier-Stokes (RANS) codes. These grids include the wind-tunnel model configuration with and without the canards in order to determine the effect of the canards in preliminary analyses. Inviscid, steady, rigid solutions have been computed by the KTH group at several test conditions in order to determine the aerodynamic loads at those conditions. Presented in Figure 26 is a sample image of the grid and pressure distributions for the wind-tunnel model configuration with canards at M=0.87 and 7 degrees angle of attack.

Using the unstructured grid generated at KTH, NASA has also generated inviscid, steady, rigid solutions at M=0.7 and 0 degrees angle of attack for the configuration with canards. Presented in Figure 27 is an image of the pressure distributions at this condition using the NASA-Langley-developed FUN3D RANS CFD code. Several additional analyses are

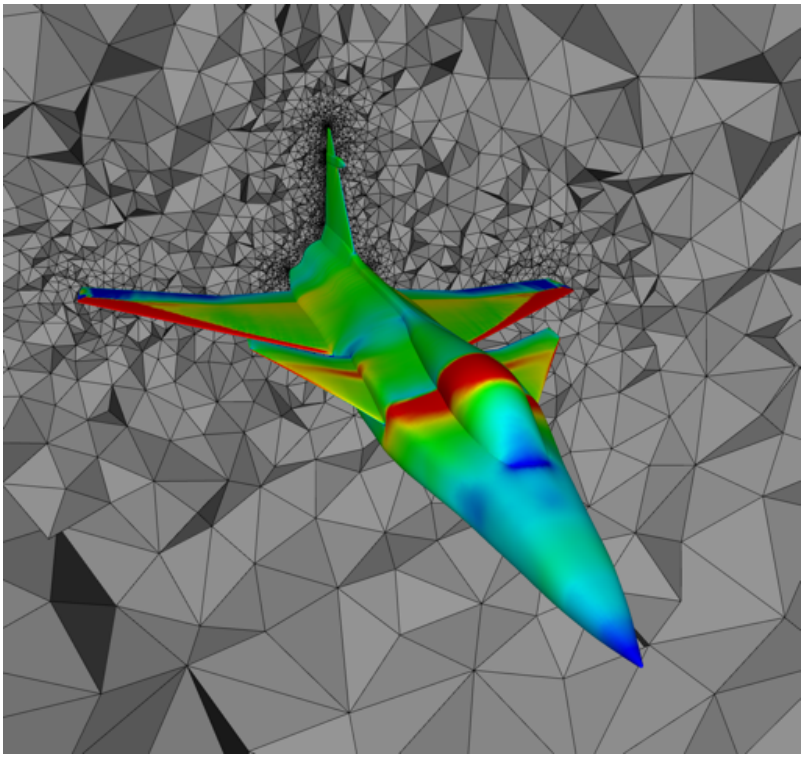

Figure 26: The CFD mesh of the wind-tunnel model with canards and steady pressures of the KTH-NASA aeroelastic wind-tunnel model at M=0.87, AoA=7 degrees.

underway at several other test conditions as well as preparation for CFD-based aeroelastic analyses.

VI. Concluding Remarks

A status review for the ASE element under the CST Project was presented. Results presented included computational aeroelastic and sonic boom propagation analysis using the FUN3D CFD code. Results presented included the effects of viscosity on the sonic boom propagation. Aeroelastic root locus plots generated using ROMs at multiple Mach numbers were presented as well. Based on these root locus plots, there are indications that the aeroelastic mechanisms exhibit some variance across Mach numbers. Finally, a brief description of a collaboration between the Royal Institute of Technology (KTH) in Stockholm, Sweden and NASA to design, fabricate, and test a full-span aeroelastic wind-tunnel model was presented.

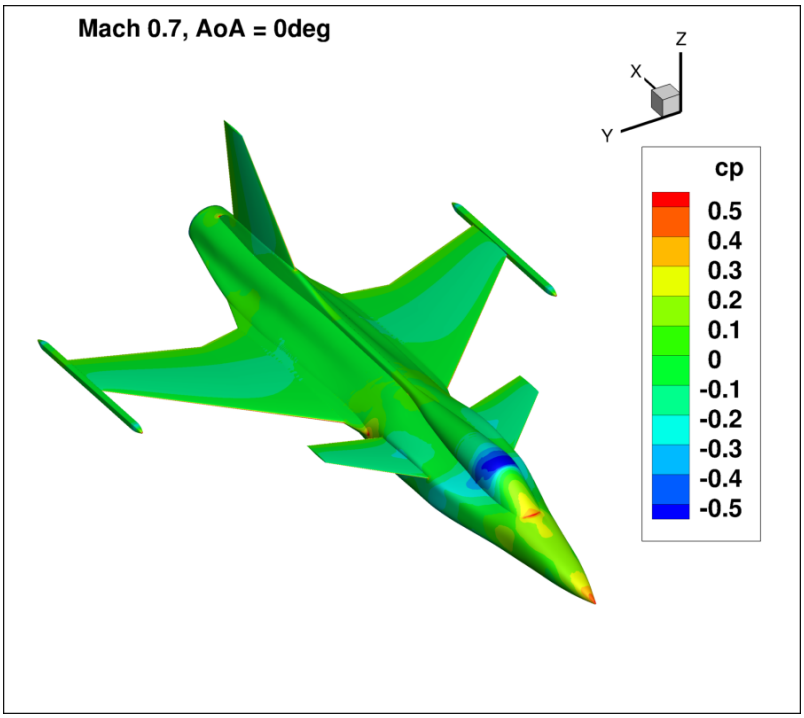

Figure 27: Pressure distributions at M=0.9, AoA=0 degrees using FUN3D code.

References

[1]Silva, W. A., Sanetrik, M. D., Chwalowski, P., Connolly, J., and Kopasakis, G., "Using FUN3D for Aeroelastic, Sonic Boom, and AeroPropulsoServoElastic (APSE) Analyses of a Supersonic Configuration," *57th AIAA/ASCE/AHS/SC Structures, Structural Dynamics, and Materials Conference*, No. 2016-1319, Jan. 2016.

[2]Silva, W. A., Garza, A. D. L., Zink, P. S., Bounajem, E., Johnson, C., Buonanno, M., Sanetrik, M. D., Chwalowski, P., Y.Yoo, S., and Hur, J., "An Overview of the NASA High Speed ASE Project: Aeroelastic Analyses of a Low-Boom Supersonic Configuration," *56th AIAA/ASCE/AHS/SC Structures, Structural Dynamics, and Materials Conference*, No. 2015-0684, Jan. 2015.

[3]Silva, W. A., Garza, A. D. L., Zink, P. S., Bounajem, E., Johnson, C., Buonanno, M., Sanetrik, M. D., Yoo, S., Kopasakis, G., and Christhilf, D. M., "The NASA High Speed ASE Project: Computational Analyses of a Low-Boom Supersonic Configuration," *55th AIAA/ASMe/ASCE/AHS/SC Structures, Structural Dynamics, and Materials Conference*, No. 2014-0675, Jan. 2014.

[4]Biedron, R. T. and Thomas, J., "Recent Enhancements to the FUN3D Flow Solver for Moving-Mesh Applications," *47th AIAA Aerospace Sciences Meeting*, No. 2009-1360, Orlando, FL, Jan. 5-8 2009.

[5]Biedron, R. T., Carlson, J.-R., Derlaga, J. M., Gnoffo, P. A., Hammond, D. P., Jones, W. T., Kleb, B., Lee-Rausch, E. M., Nielsen, E. J., Park, M. A., Rumsey, C. L., Thomas, J. L., and Wood, W. A., "FUN3D Manual: 12.8," *NASA TM-2015-218807*, 2015.

[6]Rallabhandi, S. K., "Advanced Sonic Boom Prediction Using Augmented Burger's Equation," *Journal of Aircraft*, Vol. 48, No. 4, September-October 1993, pp. 1245–1253.

[7]Silva, W. A., "Simultaneous Excitation of Multiple-Input/Multiple-Output CFD-Based Unsteady Aerodynamic Systems," *Journal of Aircraft*, Vol. 45, No. 4, July-August 2008, pp. 1267–1274.

[8]Silva, W. A., Vatsa, V. N., and Biedron, R. T., "Reduced-Order Models for the Aeroelastic Analyses of the Ares Vehicles," AIAA Paper No. 2010-4375, presented at the 28th AIAA Applied Aerodynamics Conference, Chicago, IL.

[9]Patil, M., "Limit-Cycle Oscillations of Aircraft Caused by Flutter-Induced Drag," *AIAA Journal of Aircraft*, Vol. 41, May 2004, pp. 571–576.

[10]Gopinath, A., Beran, P., and Jameson, A., "Comparative Analysis of Computational Methods for Limit-Cycle Oscillations," *47th AIAA/ASME/ASCE/AHS/ASC Structures, Structural Dynamics, and Materials Conference*, April 2006.

[11]Gordnier, R. E., "Computation of Limit-Cycle Oscillations of a Delta Wing," *AIAA Journal of Aircraft*, Vol. 40, Nov. 2003, pp. 1206–1208.

[12]Denegri, C. M., Dubben, J. A., and Maxwell, D. L., "In-Flight Wing Deformation Characteristics During Limit Cycle Oscillations," *AIAA Journal of Aircraft*, Vol. 42, March 2005, pp. 500–508.

[13]Padmanabhan, M. A., Pasiliao, C. L., and Dowell, E. H., "Simulation of Aeroelastic Limit-Cycle Oscillations of Aircraft Wings with Stores," *AIAA Journal*, Vol. 52, Oct. 2014, pp. 2291–2299.

[14]Bunton, R. W. and Denegri, C. M., "Limit Cycle Oscillation Characteristics of Fighter Aircraft," *AIAA Journal of Aircraft*, Vol. 37, Sept. 2000, pp. 916–918.

[15]Yao, W. and Marques, S., "Prediction of Transonic Limit-Cycle Oscillations Using an Aeroelastic Harmonic Balance Method," *AIAA Journal*, April 2015.

[16]Sheta, E. F., Harrand, V. J., Thompson, D. E., and Strganac, T. W., "Computational and Experimental Investigation of Limit Cycle Oscillations of Nonlinear Aeroelastic Systems," *AIAA Journal of Aircraft*, Vol. 39, Jan. 2002, pp. 133–141.

[17]Bendiksen, O., "Transonic Limit Cycle Flutter/LCO," *45th AIAA/ASME/ASCE/AHS/ASC Structures, Structural Dynamics and Materials Conference*, April 2004.

[18]Silva, W., Brenner, M., Cooper, J., Denegri, C., Dunn, S., Huttsell, L., Kaynes, I., Lind, R., Poirel, D., and Yurkovich, R., "Advanced Flutter and LCO Prediction Tools for Flight Test Risk and Cost Reduction - An International Collaborative Program for T&E Support," *2005 U.S. Air Force T&E Days*, Dec. 2005.

[19]Chabalko, C., Hajj, M., Mook, D., and Silva, W., "Characterization of the LCO Response Behaviors of the NATA model," *47th AIAA/ASME/ASCE/AHS/ASC Structures, Structural Dynamics, and Materials Conference*, April 2006.

[20]Silva, W. and Dunn, S., "Higher-Order Spectral Analysis of F-18 Flight Flutter Data," *46th AIAA/ASME/ASCE/AHS/ASC Structures, Structural Dynamics and Materials Conference*, April 2005.

[21]Corliss, J. M. and Cole, S. R., "Heavy Gas Conversion of the NASA Langley Transonic Dynamics Tunnel," *Proceedings of the 20th Advanced Measurements and Ground Testing Technology Conference*, No. 98-2710, Albuquerque, NM, June 1998.

[22]Cole, S. R. and Rivera Jr, J. A., "The New Heavy Gas Testing Capability in the NASA Langley Transonic Dynamics Tunnel," *Royal Aeronautical Society Wind Tunnels and Wind Tunnel Test Techniques Forum*, No. No. 4, Cambridge, UK, April 1997.